Journal of Chemistry and Technologies, 2024, *32*(3), 815-825

Journal of Chemistry and Technologies

pISSN 2663-2934 (Print), ISSN 2663-2942 (Online).

journal homepage: http://chemistry.dnu.dp.ua
*editorial e-mail:*chem.dnu@gmail.com

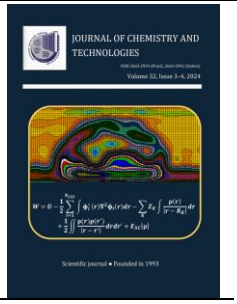

UDC 621.9

BEHAVIOUR OF ERYING-POWELL FLUID + NANOFLUID PARTICLES FLOW PAST A VERTICAL CONE IN THE PRESENCE OF MHD, SUCTION/INJECTION, HEAT AND MASS TRANSFER

Bathula Nagaraju*, Naikoti Kishan
Department of Mathematics, University College of Science, Osmania University, India
Received 1 May September 2024; accepted 9 August 2024; available online 20 October 2024

Abstract

This study investigates the flow and heat and mass transfer characteristics of a nanofluid containing Erying-Powell fluid particles over a vertical cone in the presence of magnetic field, convective boundary condition and suction/injection effects. By using appropriate similarity transformations, the controlling non-linear partial differential equations (PDEs) are converted into ordinary differential equations (ODEs). The finite element method is then used to numerically solve the resultant system of ODEs. In any flow shape, the approach may be used to offer an approximate solution to various fluid rheology problems. Graphs are used to show how different important factors affect the velocity, temperature, and concentration profiles. For vertical cone shape, the skin-friction coefficient, heat transfer rate, and mass transfer rate are also calculated and shown in tables. Finally, the graphs and tables present a comparative study of the vertical cone results. Therefore, in any flow shape, the approach may be used to offer an approximate solution to various fluid rheology problems.
*Keywords:*Eyring Powell fluid; Suction/Injection; Vertical Cone; Convective boundary condition; Magneticfield; Heattransfer; Mass transfer.

ПОВЕДІНКА РІДИНИ ЕРІНГА-ПАУЕЛЛА ТА ЧАСТИНОК НАНОРІДИНИ ПІД ЧАС ПРОТІКАННЯ ПОВЗ ВЕРТИКАЛЬНИЙ КОНУС ЗА НАЯВНОСТІ MHD, ВСМОКТУВАННЯ/НАГНІТАННЯ, ТЕПЛО- ТА МАСОПЕРЕНОСУ

Батула Наґараджу, Найкоті Кішан
Кафедра математики, Університетський науковий коледж, Університет Османія, Індія.

Анотація

У цій роботі досліджено характеристики течії та тепломасообмінунанорідини, що містить частинки рідини Ерінга-Пауелла, над вертикальним конусом за наявності магнітного поля, конвективної граничної умови та ефектів всмоктування/інжекції. За допомогою відповідних перетворень подібності керуючі нелінійні диференціальні рівняння в часткових похідних (PDE) перетворюються на звичайні диференціальні рівняння (ODE). Метод кінечних елементів використовується для чисельного розв'язання отриманої системи рівнянь. За будь-якої формі потоку цей підхід може бути використаний для наближеного розв'язання різних задач реології рідини. Графіки використовуються для демонстрації впливу різних важливих факторів на профілі швидкості, температури і концентрації. Для форми вертикального конуса також розрахованітанаведені в таблицях коефіцієнти поверхневого тертя, швидкість теплопередачі і швидкість масопередачі. Нарешті, графіки і таблиці представляють порівняльне дослідження результатів для вертикального конуса. Таким чином, за будь-якої форми потоку цей підхід може бути використаний для наближеного розв'язання різних задач реології рідини.
Ключові слова: рідина Айрінга-Пауелла; всмоктування/нагнітання; вертикальний конус; конвективна гранична умова; магнітне поле; теплопередача; масопередача.

**Correspondingauthor: e-mail: bnag2014@gmail.com*

doi: 10.15421/jchemtech.v32i3.303090

Journal of Chemistry and Technologies, 2024, *32*(3), 815-825

Introduction

In the realm of this comprehensive study, both computational simulations and empirical investigations of Eyring-Powell nanofluids flowing around a vertical cone are meticulously integrated. The examination of temperature gradients, flow rates, and pressure distributions is systematically executed through the application of experimental methodologies. By employing computational fluid dynamics (CFD) techniques, the governing equations that dictate fluid flow and heat transfer are numerically resolved, thereby ensuring a higher degree of accuracy.The exploration of Eyring-Powell nanofluids' behavior on a vertical cone offers valuable insights that could potentially revolutionize heat transfer methodologies in numerous engineering domains. Beyond fostering the development of innovative materials with enhanced properties, this research also paves the way for the creation of efficient cooling systems and solutions for thermal management.A profound understanding of the rheological characteristics of the fluid, the dynamics of heat transmission, and the effects of nanoparticle dispersion are crucial prerequisites for investigating the flow of Eyring-Powell nanofluids along a vertical cone. To delve deeper into the principles governing fluid flow and heat transfer, researchers scrutinize a multitude of parameters, such as thermal conductivity, fluid viscosity, cone angle, and nanoparticle concentration.

This research endeavor aims to shed light on the intricate interplay between fluid dynamics, heat transfer, and nanoparticle behavior, ultimately contributing to the advancement of engineering applications and the development of cutting-edge technologies. Powell and Erying [1] said that their concept included an analysis of the underlying mechanics of the relaxation theory of viscosity. The pseudo-plastic behavior in the Powell-Eyring fluid model represents the non-linear viscosity effect in the Eyring-Powell fluid flow around a sphere, as Ziegenhagen [2] pointed out. However, there is an extra viscoelastic effect in the Oldroyd fluid model, which leads to a larger deviation from Stoke's law. Ziegenhagen witnessed that. An analysis was conducted by Nadeen and Saleem [3] on the mixed convection flow of an Erying-Powell fluid along a rotating cone.

Ara et al. [4] provided illustrations of Powell-Erying flow occurring on a revolving disk and on a horizontal melting surface. The flow of an Eyring-Powell fluid may be affected by buoyancy as well as catalytic surface reactions on the upper horizontal surface of a paraboloid of revolution, as found by Abegunrin et al. [5]. Gireesha et al.'s study [6] looked at the magnetohydrodynamic (MHD) flow of a three-dimensional Eyring-Powell fluid across a stretched surface. The impacts of heat radiation and convective boundary conditions were the primary focus of the investigation. Akbar et al.'s study [7] explored the idea of an Eyring-Powell fluid on a stretched surface exposed to a magnetic field. Khan et al. [8] discussed their research on the homogenous-heterogeneous reactions in the flow of Eyring-Powell nanofluid. The existence of self-similar solutions for the Eyring-Powell fluid flow across a moving surface was investigated by Jalil et al. [9]. Referring to [10] and [11], Hayat and colleagues studied the comparison of series and numerical solutions for Eyring-Powell fluid. Additionally, the Soret and Dufour effects were studied in relation to the effects of thermal radiation and joule heating on the flow of Eyring-Powell fluid. Rehman et al. studied mixed convection and heat generation/absorption in the flow of a dual stratified Eyring Powell fluid across a stretched cylinder. The finite element solutions for MHD driven problem solving system were given by [12–31]. The works mentioned in the literature [32–38] had a significant impact on understanding the essence of the reported work.

The primary objective of this research is to investigate the flow characteristics of a two-dimensional Erying-Powell fluid in conjunction with a nanofluid under the influence of magnetohydrodynamics (MHD). The flow is directed along a vertical cone and is subject to convective boundary conditions, mass transfer, heat transfer, suction/injection, and a magnetic field. This study builds upon previous research, providing a deeper understanding of these flow-related elements.To achieve this, we utilize the fundamental Navier-Stokes Equation and the Erying-Powell fluid model to derive the governing equations. Through the application of required similarity transformations, we obtain ordinary differential equations (ODEs). We then solve these ODEs computationally using the finite element method.Our study presents the influence of various physical characteristics on the profiles of temperature, velocity, and concentration, as demonstrated through graphs and tables. This research contributes to the broader understanding of the complex interactions between Erying-Powell fluids, nanofluids, and

Journal of Chemistry and Technologies, 2024, *32*(3), 815-825

magnetohydrodynamics, providing valuable insights for experts in the field.In line with the goal, the following research questions are addressed in this study:

a) How does Erying-Powell fluid flow behave when nanofluid particles are added?

b) How do the buoyancy forces work to accelerate the Erying-Powell fluid in a given direction?

c) How do Brownian motion effects, thermophoresis, convective boundary conditions, and Prandtl number affect the temperature of Erying-Powell fluid at the wall and the rate of heat transfer?

d) How does the concentration of Erying-Powell fluid near the wall vary depending on the thermophoresis, Brownian motion, and Schmidt number?

Mathematical Formulation

The purpose of this work is to investigate the influence that heat transfer and mass transfer have on the flow of Erying-Powell + nanofluid around a vertical cone under conditions of suction/injection and convective boundary. The flow may be circular in nature, since it goes around the cone. This problem is depicted in Figure 1, which shows the specific physical position and geometry of the issue. Several presumptions have been made about this project, including the following:

a) Geometries' boundary surfaces are imposed under convective conditions.

b) Other factors taken into account are thermophoretic effects and Brownian motion.

c) The energy and concentration formulae fail to account for double diffusion effects.

d) The surface's stretching velocity, temperature and the concentration are taken as $u_w = \frac{xv}{L^2}$, $T_w = T_\infty + ax^{r_1}$, $C_w = C_\infty + ax^{r_2}$

e) α determines the cone's half angle.

Encouraging two-dimensional, electrically conducting, incompressible Erying-Powell-nanofluid flow boundary layer equations may be found by using the following assumptions:

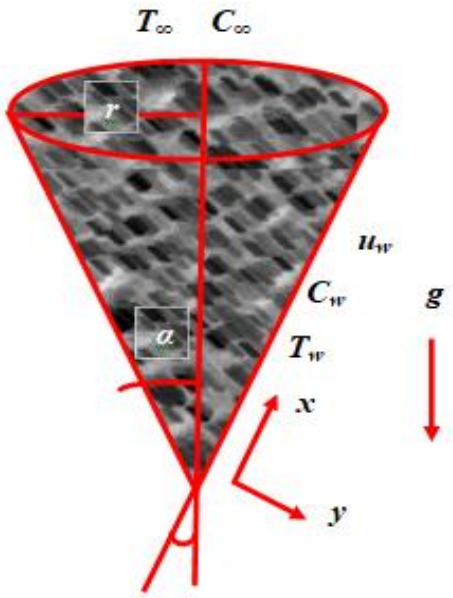

Fig. 1. The fluid flow`s geometric depiction

Continuity Equation*:*

$$\left[\frac{\partial u}{\partial x}\right]+\left[\frac{\partial v}{\partial y}\right]=0, \tag{1}$$

Momentum Equation:

$$u\left[\frac{\partial u}{\partial x}\right]+v\left[\frac{\partial u}{\partial y}\right]=\left\{\left[v+\frac{1}{\rho_f \chi C^*}\right]-\left[\frac{1}{2\rho_f \chi C^{*3}}\right]\left[\frac{\partial u}{\partial y}\right]^2\right\}\left[\frac{\partial^2 u}{\partial y^2}\right]-\left[\frac{\sigma B_o^2}{\rho_f}\right]u \tag{2}$$

$$+g\left[\left(1-C_\infty\right)\rho\beta_T\left(T-T_\infty\right)-\beta_C\left(\rho_p-\rho_f\right)\left(C-C_\infty\right)\right]\cos\alpha,$$

Equation of thermal energy:

Journal of Chemistry and Technologies, 2024, *32*(3), 815-825

$$u\left[\frac{\partial T}{\partial x}\right]+v\left[\frac{\partial T}{\partial y}\right]=\alpha^{*}\left[\frac{\partial^{2}T}{\partial y^{2}}\right]+\tau_{B}\left\{D_{B}\left[\frac{\partial C}{\partial y}\right].\left[\frac{\partial T}{\partial y}\right]+\frac{D_{T}}{T_{\infty}}.\left[\frac{\partial T}{\partial y}\right]^{2}\right\}, \tag{3}$$

Equation of species nanoparticle volume concentration:

$$u\left[\frac{\partial C}{\partial x}\right]+v\left[\frac{\partial C}{\partial y}\right]=D_{B}\left[\frac{\partial^{2}C}{\partial y^{2}}\right]+\left[\frac{D_{T}}{T_{\infty}}\right]\left[\frac{\partial^{2}T}{\partial y^{2}}\right], \tag{4}$$

These are the flow's boundary conditions

$$\left.\begin{array}{l} u=u_{w},\ v=-v_{w}(x),\ -k^{*}\left(\dfrac{\partial T}{\partial y}\right)=h_{1}\left(T_{w}-T\right),\ D_{B}\left(\dfrac{\partial C}{\partial y}\right)+\dfrac{D_{T}}{T_{\infty}}\left(\dfrac{\partial T}{\partial y}\right)=0\ \ at\ \ y=0 \\ u\to 0,\ T\to T_{\infty},\ C\to C_{\infty}\ \ as\ \ y\to\infty \end{array}\right\}, \tag{5}$$

Introducing the following similarity transformations

$$\left.\begin{array}{l} u=\dfrac{xv}{L^{2}}f'(\eta),\ v=-\dfrac{v}{L}f(\eta),\ \theta=\dfrac{T-T_{\infty}}{T_{w}-T_{\infty}},\ \phi=\dfrac{C-C_{\infty}}{C_{w}-C_{\infty}},\ \eta=\dfrac{y}{L} \end{array}\right\}, \tag{6}$$

Following the actualization of equation (1) by (6), equations (2), (3), and (4) will take on the following forms.

$$(1+\beta)f'''-\beta\lambda f'''f''^{2}+ff''-\left(f'^{2}\right)-Mf'+Gr\theta\cos\alpha+Gc\phi\cos\alpha=0, \tag{7}$$

$$\theta''+\Pr f\theta'-\Pr r_{1}f'\theta+\Pr Nb\theta'\phi'+\Pr Nt\left(\theta'\right)^{2}=0, \tag{8}$$

$$Nb\phi''+Scf\phi'-Scr_{2}f'\phi+ScNt\theta''=0, \tag{9}$$

The corresponding boundary conditions (5) become

$$\left.\begin{array}{l} f(0)=S,\ f'(0)=1,\ \theta'(0)=Bi\left[\theta(0)-1\right],\ Nb\phi'(0)+Nt\theta'(0)=1 \\ f'(\infty)\to 0,\ \theta(\infty)\to 0,\ \phi(\infty)\to 0 \end{array}\right\}, \tag{10}$$

The following are the associated physical parameters

$$\left.\begin{array}{l} M=\dfrac{2\sigma B_{o}^{2}L}{\rho_{f}},\ \Pr=\dfrac{\alpha}{\mu C_{p}},\ Nb=\dfrac{\tau D_{B}\left(C_{w}-C_{\infty}\right)}{v},\ Nt=\dfrac{\tau D_{T}\left(T_{w}-T_{\infty}\right)}{vT_{\infty}},\ We=\dfrac{\sqrt{2}\,\Gamma}{L}u_{w}, \\ Bi=\dfrac{Lh_{1}}{k^{*}},\ Gr=\dfrac{gL^{2}\beta_{T}\left(T_{w}-T_{\infty}\right)}{vu_{w}},\ Gc=\dfrac{gL^{2}\beta_{C}\left(C_{w}-C_{\infty}\right)}{vu_{w}},\ S=\dfrac{v_{w}L}{v}, \end{array}\right\}, \tag{11}$$

Quantities of physical interest, the physical parameters of the skin-friction coefficient, local Nusselt number and local Sherwood number are presented as follows:

$$Cf=C_{f}\left(\sqrt{\mathrm{Re}_{x}}\right)=\frac{\tau_{w}}{\rho u_{w}^{2}}=\left\{(1+\beta)f''(0)-\frac{1}{3}\beta\lambda f''^{3}(0)\right\} \tag{12}$$

$$Nu=\frac{xq_{w}}{\kappa\left(T_{w}-T_{\infty}\right)}=\frac{\left\{-x\left(\dfrac{\partial T}{\partial y}\right)\right\}_{y=0}}{\kappa\left(T_{w}-T_{\infty}\right)}=-\theta'(0) \tag{13}$$

$$Sh=\frac{xJ_{w}}{D_{B}\left(C_{w}-C_{\infty}\right)}=\frac{\left\{-x\left(\dfrac{\partial C}{\partial y}\right)\right\}_{y=0}}{D_{B}\left(C_{w}-C_{\infty}\right)}=-\phi'(0) \tag{14}$$

Finite Element Method Solutions.

The finite element approach is essential for solving both partial and ordinary differential equations. This approach makes it possible to solve differential equations very efficiently. The finite element approach is based on the idea that the domain may be split into smaller units called finite elements, which have a limited number of dimensions. Currently, this technique is regarded as the most adaptable and adaptive approach for doing engineering analysis. This approach has been used to investigate several fields of research, including heat conduction, hydrodynamics, solid object motion, solid mechanics, chemical processes, electrical networks, and sound propagation.

Journal of Chemistry and Technologies, 2024, *32*(3), 815-825

Figure 2 illustrates the use of the finite element approach. Prior to initiating finite element analysis, it is important to thoroughly execute the following stages:

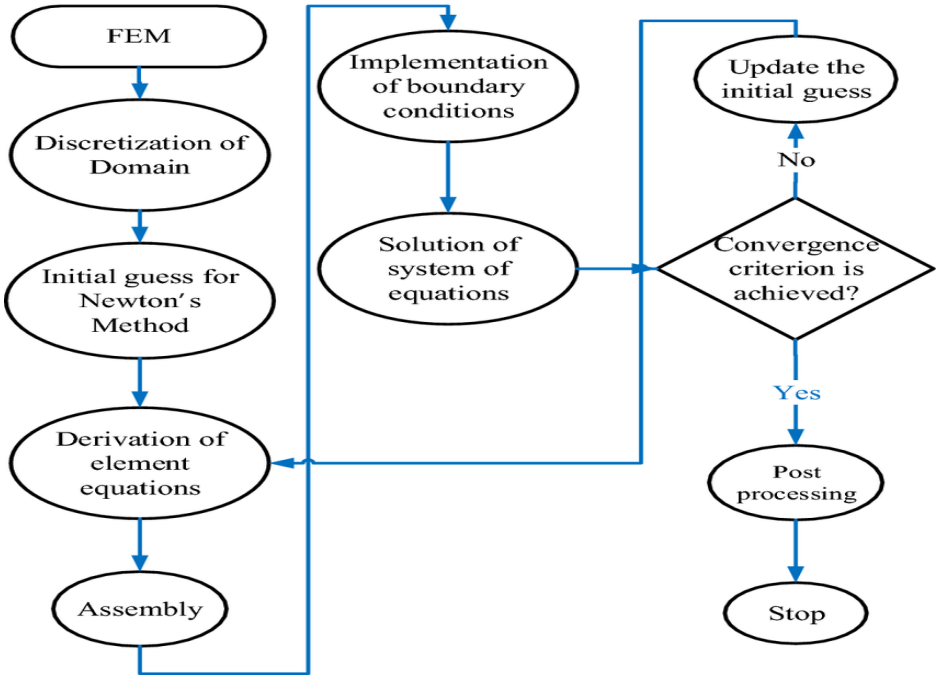

Fig. 2. Finite Element Method flow chart

Various methods, such as LU decomposition and Gauss elimination, may be used to derive numerical solutions for built equations. It is essential to consider the mathematical formulae used to approximate real functions while working with real numbers. There are 20,001 nodes in the flow domain, and each one is divided into 10,000 identically sized quadratic components. There are 10,000 identically sized quadratic components in the flow domain. Eighty thousand nonlinear equations were available for analysis once the element equations were created. Using the Gauss elimination method, the remaining system of nonlinear equations is numerically solved with an accuracy of 0.00001 once the boundary conditions have been applied. Gaussian quadrature is a very efficient technique for resolving challenges related to integration.

Program Code Validation

To ensure the accuracy and validity of the existing model, a comparison was made with the results obtained previously in [39] and [40], which are presented in Tables 1 and 2.

Table 1

Skin friction: Comparison results with [39] and [40] for the variation of r1 are presented

r_1	results of reference [39]	results of reference [40]	Results of this study
- 2.1	0.155592	0.155592	0.156356765096553
2.0	0.156001	0.155995	0.157417082750226

Table 2

Analysis of the current results of Nusselt number determination when r1 is changed in comparison with published results [39] and [40].

r_1	results of reference [35]	results of reference [36]	Results of this study
- 2.1	2.237475	2.238739	2.247680756147360
2.0	2.232780	2.234070	2.239960961456902

Results and Discussion

Compared to the results obtained in the above section after solving the equations using FEM, this section is specifically designed to specifically address the conclusions of this study and investigate the effects of various important parameters on the distributions such as velocity, temperature, and concentration. The significance and unique discoveries identified above are detailed in the following tables and figures.

The influence of fluid variable β on velocity profiles is examined in Fig. 3. It can be observed that an increase in β leads to an increase in velocity and layer thickness. From the physical

Journal of Chemistry and Technologies, 2024, *32*(3), 815-825

point of view, it can be seen that as β increases, the viscosity decreases and the fluid velocity increases.

The fluctuations of the magnetic field parameter (M) on velocity profiles are shown in Fig. 4. The Lorentz force is a resistive force that occurs when M rises and is comparable to the drag force. The Lorentz force slows motion by delaying the intensity of velocity.

The impact of the thermal Grashof number (Gr) on the cone velocity distribution is shownin Fig. 5. A higher Grashof number improves the cone's velocity dispersion. Due to the decrease in the viscosity of the nanofluid caused by the increase in the thermal Grashof number, the thickness of the boundary layerdecreases. Consequently, the velocity distribution increases as the nanofluid flow's viscosity decreases.

The effect of the solutalGrashof number (Gc) on the velocity distribution is shownin Fig. 6. This illustrates the solutalGrashof number reaction that is comparable to the thermal Grashof number. Furthermore, the phenomenon lacks both solutal buoyant forces and thermal forces when Gr = 0 and Gc = 0. Fluid flow is controlled by the suction/injection parameter. It is clear that profiles get thinner at higher S velocity values (Fig. 7). The fluid closest to the boundary rises in S<0 (injection), leading to an increase in the flow velocity and molecular collisions, ultimately resulting in an increase in internal kinetic energy. However, when S>0 (suction) occurs, the fluid close to the boundary is drawn in, resulting in porosity close to the border and a decrease in the velocity profile.

Fig. 8 illustrates how the Prandtl number (Pr) affects temperature profiles. A drop in temperature is indicated by elevated Prandtl number Pr readings over a specific threshold. We see a cooling effect when we reverse the Prandtl number and thermal diffusivity.

The temperature and concentration curves are impacted by Nb, as shown in Figs. 9 and 10. An increase in the Brownian motion parameter caused the temperature profile to settle at higher levels. The random motion caused by the collisions between base fluid and nanoparticles is known as Brownian motion. More collisions occur when the Brownian motion parameter is greater. The fluid's internal kinetic energy rises as a result of particle collisions. The concentration profile and the Brownian motion parameter have the opposite connection. The quantity of nanoparticles in the base fluid decreases as the Brownian motion parameter increases.

Temperature and concentration profiles are affected by the thermophoresis parameter (Nt), as shown in Figs. 11 and 12. As Nt values rise, so do the temperature and concentration curves. The transport force caused by the temperature differential between the fluid's layers is known as thermophoresis. Additional Thermophoresis parameter indicates that when the temperature differential between the layers rises, the rate of heat transformation correspondingly rises. The concentration of the fluid rises as the number of nanoparticles increases. Nt increases concentration profiles as well as temperature profiles as more nanoparticles transfer heat between the layers.

The thermal Biot number (Bi) and temperature distributions are directly correlated, as shown in Fig. 13. The temperature profile rises with increasing thermal Biot number values, as Fig. 13 illustrates. The coefficient of heat transport is included in the thermal biot number. No heat transmission from the wall is indicated by Bi = 0. The temperature profile rises when the thermal biot number (Bi>0) increases because of an increase in mean heat transfer rate.

Schmidt number (Sc) and concentration profile are shown in Fig. 14. The profile gets thinner as the concentration of Sc rises. Given that Sc is the viscous diffusion rate divided by the molecular diffusion rate. Therefore, by increasing the viscous diffusion rate, the molecular diffusion rate may be fixed, increasing the Schmidt number.

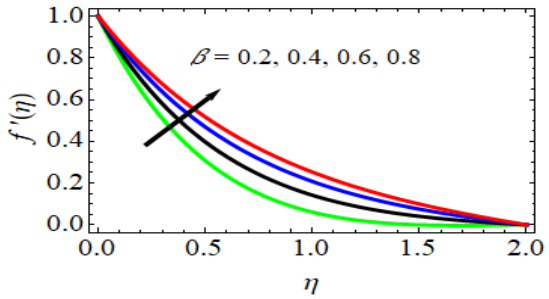

Fig. 3. *β* effect on velocity profiles

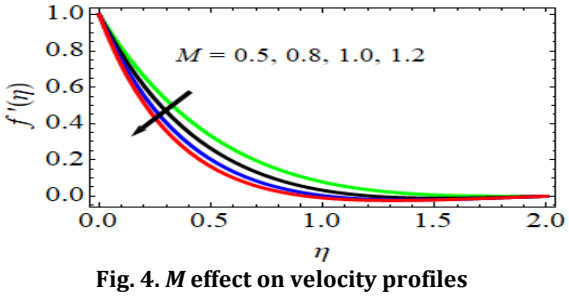

Fig. 4. *M* effect on velocity profiles

Journal of Chemistry and Technologies, 2024, *32*(3), 815-825

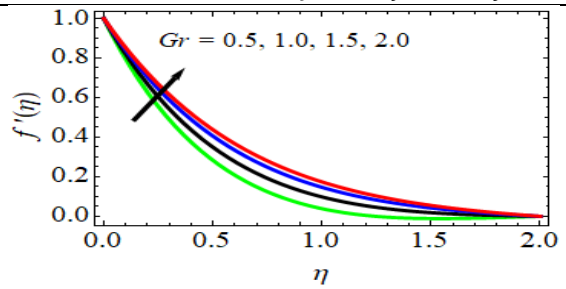

Fig. 5. *Gr* effect on velocity profiles

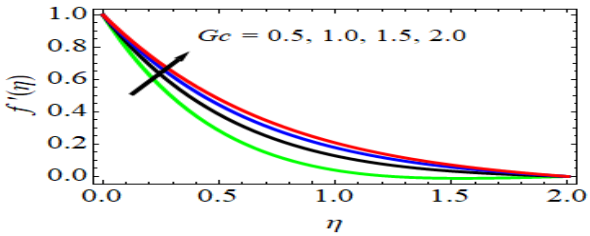

Fig. 6. *Gc* effect on velocity profiles

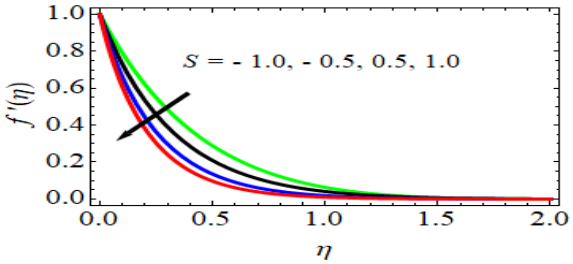

Fig. 7. *S* effect on velocity profiles

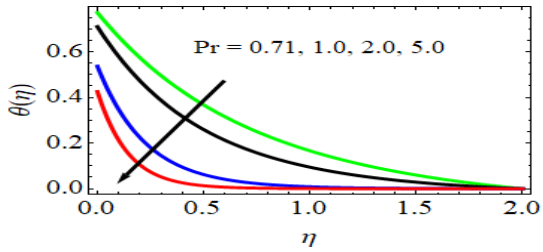

Fig. 8. Pr effect on temperature profiles

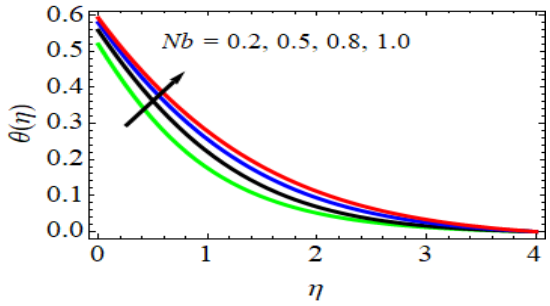

Fig. 9. *Nb* effect on temperature profiles

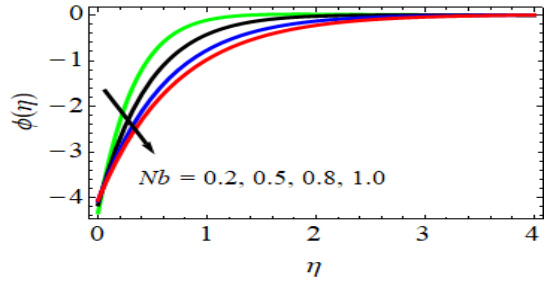

Fig. 10. *Nb* effect on concentration profiles

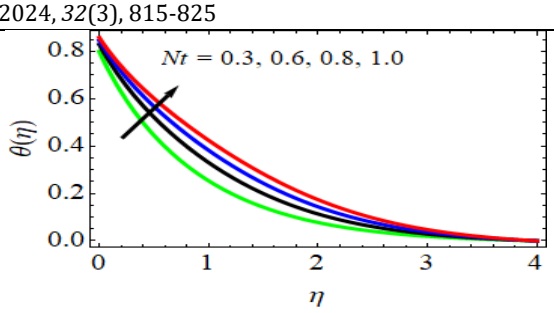

Fig. 11. *Nt* effect on temperature profiles

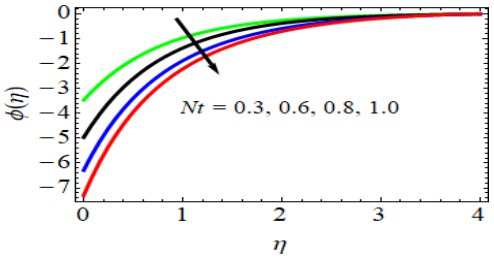

Fig. 12. *Nt* effect on concentration profiles

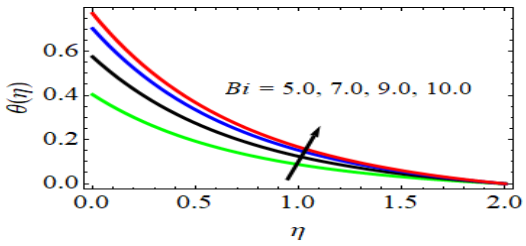

Fig. 13. *Bi* effect on temperature profiles

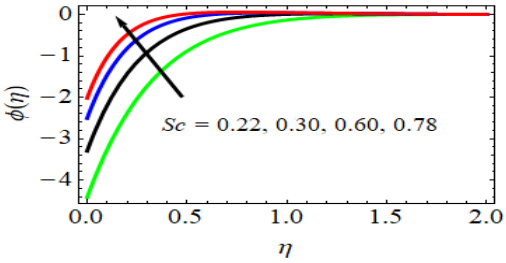

Fig. 14. *Sc* effect on concentration profiles

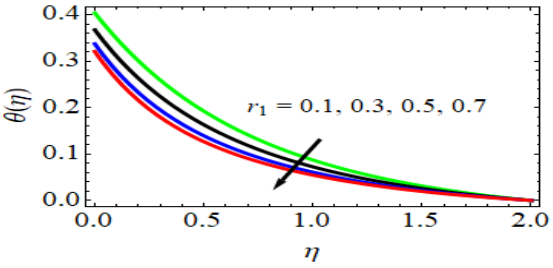

Fig. 15. r_1 effect on temperature profiles

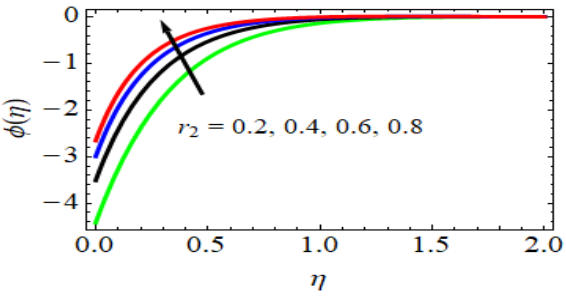

Fig. 16. r_2 effect on concentration profiles

Journal of Chemistry and Technologies, 2024, *32*(3), 815-825

Table 3

Values of skin friction with changes in parameters

β	*M*	*Gr*	*Gc*	Pr	*S*	*Bi*	r_1	r_2	*Nb*	*Nt*	*Sc*	*Cf*
0.2	0.5	0.5	0.5	0.71	- 1.0	5.0	0.1	0.2	0.2	0.3	0.22	1.457707457452
0.4												1.485758258023
0.6												1.509896456892
	0.8											1.415567608764
	1.0											1.385675676418
		1.0										1.483588542882
		1.5										1.515678071578
			1.0									1.496578728728
			1.5									1.520676767146
				1.0								1.421225876807
				2.0								1.395672726258
					- 0.5							1.426578781852
					0.5							1.408658965281
					1.0							1.375657618582
						7.0						1.486587687618
						9.0						1.518768315892
							0.3					1.431586581568
							0.5					1.415768768725
								0.4				1.420987987102
								0.6				1.407423423691
									0.5			1.476765718785
									0.8			1.490746517936
										0.6		1.482581856845
										0.8		1.501587680716
											0.30	1.401258760863
											0.78	1.375760163056

Figures 15 and 16 illustrate how wall concentration affects the temperature (r1) and concentration (r2) distributions of the cone-shaped nanofluid flow. Wall concentration is reduced by both the thermal and concentration distributions. As wall concentration increases, the thicknesses of the boundary layers decrease. This illustrates the decrease in both the temperature and concentration of the nanofluid flow.

As the values of the engineering parameters vary, Table 3 displays the numerical values of the Skin-friction coefficient. It is shown that the skin friction coefficient increases with increasing values of the following parameters in this table, but decreases with increasing values of β, M, Pr, S, r1, r2 and Sc.

It can be seen that C*f* decreases with increasing values of β, M, Pr, S, r1, r2, and Sc, while it increases with decreasing values of other parameters, as shown in table 3.

As Bi, Nb, and Nt values increase, the rate of heat transfer coefficient progressively increases; however, as Prandr1 values increase, the opposite impact is observed in table 4 . Table 5 discusses the impacts of Sc, r2, Nb, and Nt on the rate of mass transfer coefficients, or in terms of the Sherwood number coefficient. The mass transfer coefficient is shown to be growing with increasing Nt values and decreasing with increasing Sc, r2, and Nb values based on the table.

Table 4

Values of heat transfer coefficient rateat changing parameters

Pr	*Bi*	r_1	*Nb*	*Nt*	*Nu*
0.71	5.0	0.1	0.2	0.3	0.547616590645
1.00					0.515087650827
2.00					0.484657710054
	7.0				0.572188827165
	9.0				0.591875645287
		0.3			0.525676571691
		0.5			0.492257676319
			0.5		0.563658707361
			0.8		0.589265659155
				0.6	0.573881587615
				0.8	0.591756187560

Journal of Chemistry and Technologies, 2024, *32*(3), 815-825

Table5

Values of mass transfer coefficient rate at changing parameters

Sc	r_2	*Nb*	*Nt*	*Sh*
0.22	0.2	0.2	0.3	0.645716456031
0.30				0.602587680765
0.78				0.571935996131
	0.4			0.625696319155
	0.6			0.591765087680
		0.5		0.605678630185
		0.8		0.571576091760
			0.6	0.675676175135
			0.8	0.694675005761

Conclusions

This paper examines the flow toward a vertical cone of a two-dimensional, viscous, incompressible, electrically conducting magnetic fluid, taking into account mass and heat transfer. Moreover, a nanofluid is included. Conversely, Erying-Powell fluid effects were applied to the fundamental controlling partial differential equations, and similarity transformations and non-dimensional variables were used to convert them into solvable equations. The study highlights a number of important findings about the distribution of velocity, temperature, and concentration, including the effects of magnetic field, Solutal and Thermal Grashof numbers, Suction/Injection, Prandtl number, Biot number, Thermal wall concentration, Brownian motion, Thermophoresis, and Schmidt number.

A. When a magnetic field and suction or injections are present, the velocity distribution in the fluid flow decreases. In contrast, the Erying-Powell fluid parameters favorable affect – thermal and solutal Grashof numbers – lead to an increase in the velocity.

B. In contrast to the decrease inPrandtl number and thermal wall concentration parameter, the fluid flow temperature increased with thermophoresis, Brownian motion, and Biot number.

C. Schmidt number, Brownian motion coefficient, and solutal wall concentration parameter were shown to influence the lowering of the nanoparticle concentration distribution. The presence of the thermophoresis coefficient, however, had the opposite effect.

D. Lastly, a comparison of this research with [39] and [40] is presented

References

[1] Powell, R. E., Erying, H., (1994). Mechanisms for the relaxation theory of viscosity, *Nature, 154*(3909), 427–428, doi:10.1038/154427a0.

[2] Ziegenhagen, A. (1964). The very slow flow of a Powell-Eyring fluid around a sphere, *Appl. Sci. Res., 14*(1), 43–56, doi:10.1007/bf00382230.

[3] Nadeem, S., Saleem, S. (2014). Mixed convection flow of Eyring-Powell fluid along a rotating cone, *Results Phys.,* 4, 54–62, doi:10.1016/j.rinp.2014.03.004.

[4] Ara, A., Khan, N. A., Khan, H., Sultan, F. (2014). Radiation effect on boundary layer flow of an Eyring - Powell fluid over an exponentially shrinking sheet, *Ain Shams Eng. J., 5*(4), 1337–1342, doi:10.1016/j.asej.2014.06.002

[5] Abegunrin, O. A., Animasaun, I. L., Sandeep, N. (2018). Sight into the boundary layer flow of non-Newtonian Eyring-Powell fluid due to catalytic surface reaction on an upper horizontal surface of a paraboloid of revolution, *Alex. Eng. J., 57*(3), 2051–2060, doi:10.1016/j.aej.2017.05.018.

[6] Gireesha, B. J. Gorla, R. S. Reddy, B. Mahanthesh. (2015). Effect of suspended nanoparticles on three-dimensional MHD flow heat and mass transfer of radiating Eyring-Powell fluid over a stretching sheet, *J Nanofluids, 4*, 474–484.

[7] Akbar, N. S., Ebaid, A., Khan, Z. H. (2015).Numerical analysis of magnetic field effects on Eyring-Powell fluid flow towards a stretching sheet, *J. Magnet. Mater., 382*, 355–358.

[8] Khan, A., Malik, M. Y., Salahuddin, T., Khan, M., Rehman, K. U. (2017). Homogenous-heterogeneous reactions in MHD flow of Powell-Eyring fluid over a stretching sheet with Newtonian heating, *Neural Comput Appl*, 30, 3581–3588. doi:10.1007/s00521-017-2943-6.

[9] Jalil, M., Asghar, S., Imran, S. M. (2013). Self similar solutions for the flow and heat transfer of Powell-Eyring fluid over a moving surface in a parallel free stream, *Int. J. Heat Mass Transfer, 65*, 73–79.

[10] Hayat, T., Ali, S., Farooq, M.A., Alsaedi, A. (2015). On comparison of series and numerical solutions for flow of Eyring-Powell fluid with Newtonian heating and internal heat generation/absorption, *PLoS One,* doi:10.1371/journal.pone.0129613.

[11] Hayat, T., Ali, S., Alsaedi, A., Alsulami, H.H. (2016). Influence of thermal radiation and joule heating in the Eyring-Powell fluid flow with the Soret and DuFour effects, *J. Appl. Mech. Tech. Phys., 57*, 1051–1060

[12] Murali, G., Paul, A., Babu, N.V.N. (2015). Heat and mass transfer effects on an unsteady hydromagnetic free convective flow over an infinite vertical plate embedded in a porous medium with heat absorption, *Int. J. Open Problems Compt. Math, 8*(1), 15–28. doi: 10.12816/0010706

[13] Deepa, G., Murali, G. (2014). Analysis of soret and dufour effects onunsteady MHD flow past a semi infinite vertical porous plate via finite difference method, *International journal of applied physics and mathematics, 4*(5), 332–344. doi: 10.7763/IJAPM.2014.V4.306.

[14] Murali, G., Paul, A., Babu, N.V.N. (2015). Numerical study of chemical reaction effects on unsteady MHD fluid flow past an infinite vertical plate embedded in a porous medium with variable suction, *Electronic Journal of mathematical analysis and applications*, *3*(2), 179–192.

[15] Babu, N.V.N., Paul, A., Murali, G. (2015). Soret and Dufour effects on unsteady hydromagnetic free convective fluid flow past an infinite vertical porous plate in the presence of chemical reaction, *Journal of science and arts*, *15*(1), 99–111.

[16] Murali, G., Reddy, M.C.K., Sivaiah, S. (2012). Finite element solution of thermal radiation effect on unsteady MHD flow past a vertical porous plate with variable suction,*American Academic & Scholarly Research Journal, 4*(3), 3–22.

[17] Babu, N.V.N.,Murali, G., Bhati, S.M.(2018). Casson fluid performance on natural convective dissipative couette flow past an infinite vertically inclined plate filled in porous medium with heat transfer, MHD and hall current effects, *International journal of Pharmaceutical Research, 10*(4), 2018.

[18] Gundagani, M., Sheri, S., Paul, A., Reddy, M. C. K. (2013). Radiation Effects on an Unsteady MHD Convective Flow Past a Semi-Infinite Vertical Permeable Moving Plate Embedded in a Porous Medium with Viscous Dissipation, *Walailak J Sci &; Tech*, 10(5), 499–515. doi: 10.2004/wjst.v10i5.380

[19] Murali, G., Sivaiah, Sh., Paul, A., Reddy, M. C. K. (2013). Unsteady magnetohydrodynamic free convective flow past a vertical porous plate, *International journal of applied science and engineering*, *11*(3), 267–275.

[20] Murali, G. Deepa, G. Nirmala Kasturi, V, Poornakantha, T. (2023). Joint effects of thermal diffusion and diffusion thermo on MHD three dimensional nanofluid flow towards a stretching sheet, *Mathematical models in engineering*. https://doi.org/10.21595/mme.2023.23590.

[21] Gundagani, M., Babu, N.V.N., Gadially, D. (2024). Study of Nano-Powell-Erying fluid flow past a porous stretching sheet by the effects of MHD, thermal and mass convective boundary conditions. *J. Umm Al-Qura Univ. Eng. Archit.* https://doi.org/10.1007/s43995-024-00056-2

[22] Gundagani, M., Mamidi, L.P., Tanuku, P.K. (2024). Finite element solutions of Double diffusion effects on three-dimensional MHD Nano-Powell-Erying fluid flow in presence of thermal and mass Biot numbers. *J. Eng. Appl. Sci. 71*, 9 https://doi.org/10.1186/s44147-023-00347-w

[23] Deepa, G., Murali, G (2014). Effects of viscous dissipation on unsteady MHD free convective flow with thermophoresis past a radiate inclined permeable plate, *Iranian Journal of Science and Technology (Sciences)*, 38A3, DOI: 10.22099/IJSTS.2014.2437

[24] Murali, G, Babu, N.V.N. (2023). Convective MHD Jeffrey Fluid Flow Due to Vertical Plates with Pulsed Fluid Suction:A Numerical Study, *Journal of computational applied mechanics, 56*(1), 36–48. 10.22059/JCAMECH.2023.351326.773.2023.

[25] Murali, G., Babu, N.V.N. (2012). Effect of Radiation on MHD Convection Flow Past a Vertical Permeable Moving Plate, *International Journal of Advances in Applied Sciences* **(**IJAAS**),** 1(1), 19–28.

[26] Sivaaih, S., Murali, G., Reddy, M.C.K., Srinivasa R. (2012). Unsteady MHD mixed convection flow past a vertical porous plate in prsesence of radiation, *International journal of basic and applied sciences*, *1*(4), 651–666.

[27] Reddy, M.C.K., Murali, G., Sivaiah, S., Babu, N.V.N. (2012). Heat and mass transfer effects on unsteady MHD free convection flow past a vertical permeable moving plate with radiation, *International Journal of Applied Mathematical Research*, *1*(2), 189–205.

[28] Sivaiah, S., Murali, G., Reddy, M.C.K. (2012). Finite Element Analysis of Chemical Reaction and Radiation Effects on Isothermal Vertical Oscillating Plate with Variable Mass Diffusion, International Scholarly Research Network ISRN *Mathematical Physics, 2012*, 401515, doi:10.5402/2012/401515.

[29] Murali, G., Sheri, S., Reddy, M.C.K. (2012). Soret and dufour effects on unsteady mhd mixed convection flow past a verticle porous plate with thermal radiation, *Caspian journal of applied sciences research*, 1(9). doi: 10.4236/am.2012.37105

[30] Singh, N., Kaur, J., Thakur, P., Murali, G. (2023). Structural behaviour of annular isotropic disk made of steel/copper material with gradually varying thickness subjected to internal pressure, *structural integrity and life,* 23(3), 293–297.

[31] Sheri, S., Gundagani, M., Karanamu, M. P. (2012). Analysis of Heat and Mass Transfer Effects on an Isothermal Vertical Oscillating Plate.*Walailak Journal of Science and Technology (WJST)*, *9*(4),407–415. https://wjst.wu.ac.th/index.php/wjst/article/view/451

[32] Eswaramoorthi, S., Sivasankaran, S. (2022). Entropy optimization of MHD Casson-Williamson Fluid Flow over a convectively heated stretchy sheet with Cattaneo-Christov dual Flux. *Scientia Iranica*, *29*(5), 2317-2331. doi: 10.24200/sci.2022.58291.5654

[33] Prabakaran R, Eswaramoorthi S, Loganathan K, Sarris IE. Investigation on Thermally Radiative Mixed Convective Flow of Carbon Nanotubes/Al_2O_3 Nanofluid in Water Past a Stretching Plate with Joule Heating and Viscous Dissipation. *Micromachines*. 2022; 13(9):1424. https://doi.org/10.3390/mi13091424

[34] Riaz, S., Afzaal, M. F., Wang, Z., Jan, A., & Farooq, U. (2023). Numerical heat transfer of non-similar ternary hybrid nanofluid flow over linearly stretching surface. *Numerical Heat Transfer, Part A: Applications,* 1–15. https://doi.org/10.1080/10407782.2023.2251093

[35] Cui J, Jan A, Farooq U, Hussain M, Khan WA. (2022). Thermal Analysis of Radiative Darcy–Forchheimer Nanofluid Flow across an Inclined Stretching Surface. *Nanomaterials*. *12*(23), 4291. https://doi.org/10.3390/nano12234291

[36] Farooq, J., Mushtaq, M., Munir, S. *et al.* Slip flow through a non-uniform channel under the influence of transverse magnetic field. *Sci Rep 8,* 13137 (2018). https://doi.org/10.1038/s41598-018-31538-8

[37] Jan, A, Mushtaq, M, Farooq, U, Hussain, M. (2022). Nonsimilar analysis of magnetized Sisko nanofluid flow subjected to heat generation/absorption and viscous dissipation, *Journal of Magnetism and Magnetic Materials*, *564*(2), 170153 https://doi.org/10.1016/j.jmmm.2022.170153.

[38] Cui, J., Munir, Sh., Raies, S. F., Farooq, U., Razzaq, R. (2022). Non-similar aspects of heat generation in bioconvection from flat surface subjected to chemically

reactive stagnation point flow of Oldroyd-B fluid, *Alexandria Engineering Journal, 61*(7), 5397–5411, https://doi.org/10.1016/j.aej.2021.10.056.

[39] Vajravelu, K., Nayfeh, J. (1992).Hydromagnetic convection at a cone and a wedge, *Int. Commun. Heat Mass Tranf., 19,* 701–710.

[40] Chamkha, J. A. (1996). Non-Darcy hydromagnetic free convection from a cone and a wedge in porous media, *Int. Commun. Heat Mass Tranf., 23*(6), 875–887.